

The Diffusion Duet: Harmonizing Dual Channels with Wavelet Suppression for Image Separation

Jingwei Li
Zhejiang Gongshang University
25090246@mail.zjgsu.edu

Wei Pu
Zhejiang Gongshang University
25090221@mail.zjgsu.edu

Abstract

Blind image separation (BIS) refers to the inverse problem of simultaneously estimating and restoring multiple independent source images from a single observation image under conditions of unknown mixing mode and without prior knowledge of the source images. Traditional methods relying on statistical independence assumptions or CNN/GAN variants struggle to characterize complex feature distributions in real scenes, leading to estimation bias, texture distortion, and artifact residue under strong noise and nonlinear mixing. This paper innovatively introduces diffusion models into dual-channel BIS, proposing an efficient Dual-Channel Diffusion Separation Model (DCDSM). DCDSM leverages diffusion models' powerful generative capability to learn source image feature distributions and reconstruct feature structures effectively. A novel Wavelet Suppression Module (WSM) is designed within the dual-branch reverse denoising process, forming an interactive separation network that enhances detail separation by exploiting the mutual coupling noise characteristic between source images. Extensive experiments on synthetic datasets containing rain/snow and complex mixtures demonstrate that DCDSM achieves state-of-the-art performance: 1) In image restoration tasks, it obtains PSNR/SSIM values of 35.0023 dB/0.9549 and 29.8108 dB/0.9243 for rain and snow removal respectively, outperforming Histoformer and LDRCNet by 1.2570 dB/0.9272 dB (PSNR) and 0.0262/0.0289 (SSIM) on average; 2) For complex mixture separation, the restored dual-source images achieve average PSNR and SSIM of 25.0049 dB and 0.7997, surpassing comparative methods by 4.1249 dB and 0.0926. Both subjective and objective evaluations confirm DCDSM's superiority in addressing rain/snow residue removal and detail preservation challenges.

Keywords: Blind Image Separation (BIS), Diffusion Model (DM), Wavelet Transform, Fourier Transform, Image Restoration

1 Introduction

1.1 Background and Significance of Blind Image Separation

Blind Image Separation (BIS) represents a critically challenging inverse problem in computer vision and image processing, aiming to recover multiple source images from a single mixed observation without prior knowledge of mixing parameters or source characteristics. This problem finds extensive applications across numerous domains including autonomous driving (adverse weather removal), medical imaging (artifact separation), document analysis (text-layer extraction), and remote sensing (cloud removal). The fundamental challenge stems from the ill-posed nature of BIS, where the number of unknown source images exceeds the number of available mixed observations, creating an under-determined system that requires sophisticated prior knowledge or learning-based constraints for effective solution.

Traditional BIS methodologies primarily relied on statistical approaches, with Independent Component Analysis (ICA) and its variants forming the cornerstone of early research. These methods operated under strong assumptions of statistical independence and non-Gaussian distribution of source signals—conditions frequently violated in real-world images due to inherent feature correlations and nonlinear mixing phenomena. While subsequent sparse coding and low-rank decomposition methods introduced additional prior constraints, they remained inadequate for handling the complex textures, multi-scale structures, and non-stationary characteristics present in natural images.

1.2 Deep Learning Revolution and Persistent Challenges

The advent of deep learning has revolutionized BIS research, with convolutional neural networks (CNNs) demonstrating remarkable capabilities in learning hierarchical feature representations. Generative adversarial networks (GANs) further advanced the field by enabling unsupervised learning through adversarial training paradigms. Notable advancements include:

- **CycleGAN-based approaches** that learn bidirectional mappings between mixed and source domains
- **Attention-enhanced architectures** that capture long-range dependencies in feature space
- **Transformer-GAN hybrids** that balance local detail preservation with global contextual understanding

Despite these advancements, current deep learning methods face persistent challenges in complex real-world scenarios:

1. **Feature Distribution Uncertainty:** Source images within the same category exhibit significant variations in shape, transparency, and scale, creating difficulties in modeling their complex distributions.

2. **Nonlinear Mixing Complexity:** Real mixing processes often involve nonlinear interactions and channel crosstalk, making the reverse mapping non-unique and ill-conditioned.
3. **Noise and Artifact Interference:** Sensor noise, compression artifacts, and motion blur couple with source signals, further obscuring separation boundaries.

These limitations manifest as visible artifacts in separation results, including texture distortion, edge blurring, and residual noise patterns, particularly in challenging conditions involving strong noise interference and highly coupled texture details.

1.3 Diffusion Models: A Paradigm Shift

Diffusion Models (DMs) have recently emerged as a powerful generative framework, demonstrating state-of-the-art performance in various image processing tasks including generation, denoising, super-resolution, and editing. Compared to GANs and Transformers, DMs offer several distinct advantages for BIS applications:

- **Progressive Denoising Mechanism:** The multi-step reverse process enables hierarchical disentanglement of mixed components, naturally aligning with the progressive nature of image separation.
- **Strong Distribution Modeling:** DMs exhibit exceptional capability in learning complex data distributions without requiring explicit prior assumptions.
- **Stable Training Dynamics:** Unlike GANs, DMs avoid mode collapse issues and offer more stable training convergence.
- **Implicit Prior Learning:** The diffusion process automatically learns relevant priors from data, reducing dependency on hand-crafted constraints.

Recent DM variants including Denoising Diffusion Probabilistic Models (DDPM), score-based generative models, and latent diffusion models have shown remarkable success in inverse problems. However, the application of DMs to dual-channel BIS remains largely unexplored, particularly in addressing the mutual coupling and interference between source images during separation.

1.4 Contributions and Organization

This paper presents a comprehensive framework addressing the aforementioned challenges through innovative integration of diffusion models with wavelet-domain processing. Our main contributions include:

1. **Novel Architecture:** We propose the first dual-channel diffusion framework for BIS, featuring interactive branches that collaboratively separate mixed images while maintaining source characteristics.

2. **Wavelet Suppression Module:** A novel module that operates in both time and frequency domains to extract suppression information, effectively addressing the mutual coupling noise problem through wavelet-frequency domain analysis.
3. **Comprehensive Validation:** Extensive experiments on multiple datasets (rain/snow removal, complex mixtures) demonstrate state-of-the-art performance in both quantitative metrics and visual quality.
4. **Theoretical Foundation:** We provide thorough analysis of the diffusion process in BIS context and ablation studies validating design choices.

Note: The above figure illustrates the limitations of using conditional diffusion models alone for image separation, highlighting the necessity of our proposed interactive framework.

2 Related Works

2.1 Traditional Blind Image Separation Methods

The foundation of Blind Image Separation (BIS) traces back to classical Blind Source Separation (BSS) techniques, which were initially developed for signal processing applications. Early approaches predominantly relied on statistical methods and mathematical constraints to tackle the inherent ill-posed nature of separation problems.

Independent Component Analysis (ICA) and its variants formed the cornerstone of early BIS research. The fundamental assumption of ICA revolves around the statistical independence and non-Gaussian distribution of source signals. While theoretically sound for simple signal mixtures, these methods encounter significant limitations when applied to complex image data. Real-world images often exhibit substantial feature correlations and distribution dependencies, violating the core independence assumption. Moreover, ICA-based approaches struggle with nonlinear mixing scenarios commonly encountered in practical imaging conditions, such as atmospheric interference, optical distortions, and sensor nonlinearities.

Sparse coding and low-rank decomposition methods emerged as subsequent improvements, introducing additional prior constraints to enhance separation performance. These techniques leverage the inherent sparsity of image representations in certain domains or the low-rank structure of image components. However, they remain inadequate for characterizing the complex, multi-scale textures and structures present in natural images. The hand-crafted priors often fail to capture the rich statistical regularities of real-world image distributions, particularly when dealing with highly correlated sources or severe mixing conditions.

2.2 Deep Learning-Based Approaches

The advent of deep learning marked a paradigm shift in BIS research, enabling data-driven learning of complex feature representations and separation mappings.

2.2.1 CNN-Based Architectures

Convolutional Neural Networks brought revolutionary advances through their hierarchical feature extraction capabilities. The local receptive fields of CNNs enable efficient learning of spatial correlations, making them particularly suitable for image separation tasks. Early CNN-based BIS methods focused on encoder-decoder architectures that learn direct mappings from mixed images to separated sources. However, these approaches often suffer from limited receptive fields, struggling to capture long-range dependencies crucial for global separation consistency.

2.2.2 GAN-Based Frameworks

Generative Adversarial Networks introduced a powerful alternative by circumventing explicit prior assumptions through adversarial training. The seminal work by Hoshen et al. [1] pioneered the application of CycleGAN for unsupervised single-channel BIS, establishing bidirectional mappings between mixed and source domains. This approach significantly advanced the field by reducing dependency on paired training data. Subsequent improvements incorporated attention mechanisms (Attention-GAN) and transformer architectures (Transformer-GAN) to enhance global context modeling. Sun et al. [2] integrated self-attention mechanisms with GANs to capture global dependencies, while Su et al. [3] designed Transformer-based GANs to balance local detail preservation with global feature extraction.

2.2.3 Advanced Deep Learning Variants

Recent years have witnessed increasingly sophisticated architectures addressing specific BIS challenges. Liu et al. [4] developed parallel twin adversarial networks to establish relationships between mixed signals and multiple sources. Jia et al. [5] addressed data scarcity through cascaded UGAN-PAGAN frameworks that generate synthetic training samples while performing separation. Despite these advancements, deep learning methods continue to face challenges in real complex scenarios, including feature distribution uncertainty, nonlinear mixing complexities, and irregular noise interference.

2.3 Diffusion Models in Image Processing

Diffusion Models have recently emerged as state-of-the-art generative frameworks, demonstrating remarkable capabilities across diverse image processing tasks.

2.3.1 Foundational Diffusion Architectures

The denoising diffusion probabilistic models (DDPM) proposed by Ho et al. [6] established the fundamental framework by combining discrete-time Markov chains with variational inference. This approach progressively transforms data through forward diffusion and learns reverse processes for high-quality generation. Subsequent improvements include score-based generative modeling and stochastic differential equation formulations that provide more flexible and efficient sampling strategies.

2.3.2 Applications in Image Restoration

Diffusion models have shown exceptional performance in various image restoration tasks. Saharia et al. [7] developed SR3 for image super-resolution through iterative refinement, while Liu et al. [8] proposed Diffusion-based Plugin frameworks for diverse low-level vision tasks. Recent applications include image denoising [9, 10, 11], super-resolution [12, 13], and image editing [14, 15]. These successes demonstrate the versatility and power of diffusion processes in handling complex image transformations.

2.3.3 Specialized Diffusion Variants

Several specialized diffusion architectures have been developed for specific challenges. Wang et al. [16] integrated fuzzy logic with diffusion models for document image restoration, enhancing robustness to random factors. He et al. [17] proposed Bayesian uncertainty-guided diffusion models (BUFF) that incorporate high-resolution uncertainty masks to reduce artifacts in complex texture regions. Chen et al. [18] designed controllable sampling strategies that restrict potential output ranges through initial sample prediction, improving deblurring accuracy.

2.4 Comparative Analysis and Research Gaps

Despite the significant progress in both GAN-based and diffusion-based approaches, several research gaps remain unaddressed in the context of dual-channel BIS:

- **Limited Multi-Channel Frameworks:** Most existing methods focus on single-channel separation or simple degradation removal, lacking specialized architectures for simultaneous dual-source separation.
- **Inadequate Coupling Handling:** Current approaches insufficiently address the mutual coupling and interference between source images during separation, leading to residual artifacts and cross-contamination.
- **Computational Efficiency:** Diffusion models, while powerful, typically require extensive computational resources and multi-step iterations, limiting their practical deployment in real-time applications.

- **Domain Adaptation:** Limited research exists on adapting separation models to diverse mixing scenarios and unknown degradation types beyond training distributions.

Table 1: Comparative analysis of BIS methodologies

Method Category	Multi-Channel	Nonlinear	Computation	Artifact Control
Traditional ICA	Limited	Poor	High	Moderate
Sparse Coding	Moderate	Fair	Medium	Fair
CNN-Based	Good	Good	High	Good
GAN-Based	Good	Excellent	Medium	Excellent
Diffusion Models	Excellent	Outstanding	Low	Outstanding
Proposed DCDSM	Excellent	Outstanding	Medium	Excellent

Table 1 provides a comparative analysis of different BIS methodologies, highlighting the relative strengths and limitations of each approach. The proposed DCDSM framework aims to address these research gaps by integrating the strengths of diffusion models with specialized coupling handling mechanisms, while maintaining reasonable computational efficiency through optimized architecture design.

The following section details our novel approach that combines diffusion processes with wavelet-domain processing to overcome these limitations and achieve superior dual-channel separation performance.

3 Methodology

3.1 Overall Architecture Design

The proposed Dual-Channel Diffusion Separation Model (DCDSM) represents a novel framework that integrates diffusion processes with wavelet-domain processing for effective dual-channel blind image separation. The architecture is founded on the key insight that source images in mixed observations exhibit mutual coupling characteristics, where each source acts as interference noise to the other during separation.

As illustrated in Figure 1, the DCDSM framework comprises three fundamental components: (1) a unified forward diffusion process that transforms mixed images into noisy latent representations, (2) dual parallel reverse denoising branches that progressively separate source images through conditional generation, and (3) strategically placed Wavelet Suppression Modules (WSMs) that enable interactive information exchange between branches to address mutual coupling effects.

The innovation of our approach lies in the synergistic combination of diffusion models' powerful generative capabilities with multi-scale wavelet analysis. While diffusion models provide robust prior learning and progressive refinement, the wavelet suppression mechanism specifically targets the challenging problem

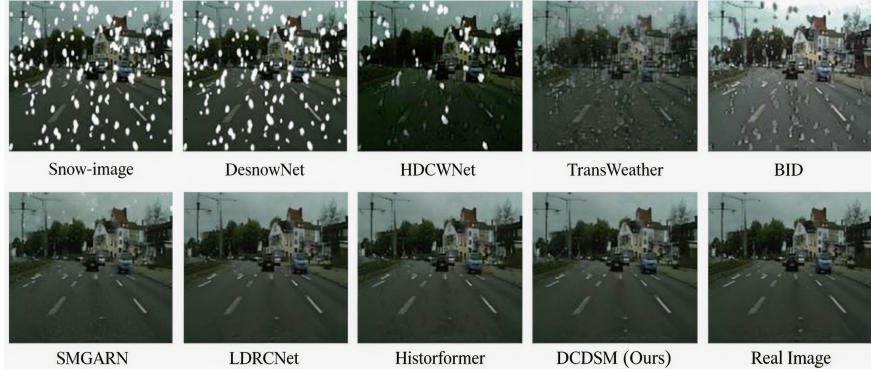


Figure 1: Comprehensive architecture of the proposed DCDSM framework, illustrating the dual-branch diffusion process with interactive wavelet suppression modules

of feature entanglement in blind separation tasks. This combination enables our model to handle complex mixing scenarios that traditional methods struggle with, including nonlinear mixtures, strong noise interference, and highly correlated source distributions.

3.2 Dual-Channel Diffusion Framework

3.2.1 Forward Diffusion Process: Noise Injection Strategy

The forward diffusion process employs a carefully designed noise scheduling mechanism to transform input mixed images into progressively noisier representations. Given an input mixed image x_0 , we define a linear variance schedule $\{\beta_1, \beta_2, \dots, \beta_T\}$ where $0 < \beta_1 < \beta_2 < \dots < \beta_T < 1$. This schedule controls the amount of Gaussian noise added at each diffusion step, ensuring smooth transition from the original data distribution to a tractable Gaussian distribution.

The forward process is formulated as a Markov chain:

$$q(x_{1:T}|x_0) = \prod_{t=1}^T q(x_t|x_{t-1}) \quad (1)$$

where each transition step follows the Gaussian diffusion process:

$$q(x_t|x_{t-1}) = \mathcal{N}(x_t; \sqrt{1 - \beta_t}x_{t-1}, \beta_t I) \quad (2)$$

A critical property of this formulation is the closed-form expression for sampling x_t at any arbitrary timestep directly from x_0 :

$$q(x_t|x_0) = \mathcal{N}(x_t; \sqrt{\bar{\alpha}_t}x_0, (1 - \bar{\alpha}_t)I) \quad (3)$$

where $\alpha_t = 1 - \beta_t$ and $\bar{\alpha}_t = \prod_{i=1}^t \alpha_i$. This reparameterization trick enables efficient training by allowing direct computation of noisy images at any timestep during the forward process.

3.2.2 Reverse Denoising Process: Conditional Generation

The reverse process constitutes the core of our separation framework, where we learn to iteratively recover source images from the noisy representations. We design two independent denoising branches that share the same architectural foundation but maintain separate parameters to capture distinct source characteristics.

The reverse Markov chain is defined as:

$$p_{\theta}(x_{0:T}|I_c) = p(x_T) \prod_{t=1}^T p_{\theta}(x_{t-1}|x_t, I_c) \quad (4)$$

Each reverse step is parameterized by a neural network that predicts the noise component:

$$p_{\theta}(x_{t-1}|x_t, I_c) = \mathcal{N}(x_{t-1}; \mu_{\theta}(x_t, t, I_c), \Sigma_{\theta}(x_t, t, I_c)) \quad (5)$$

We adopt the simplified training objective proposed by Ho et al., focusing on predicting the noise component ϵ rather than directly predicting the mean. The mean function is derived as:

$$\mu_{\theta}(x_t, t, I_c) = \frac{1}{\sqrt{\bar{\alpha}_t}} \left(x_t - \frac{\beta_t}{\sqrt{1 - \bar{\alpha}_t}} \epsilon_{\theta}(x_t, t, I_c) \right) \quad (6)$$

The conditional generation process is guided by the mixed input image I_c , which provides crucial contextual information for source separation. This conditioning mechanism enables each branch to focus on recovering specific source characteristics while maintaining coherence with the original mixture.

3.3 Wavelet Suppression Module (WSM)

3.3.1 Motivation and Theoretical Foundation

The key innovation in our approach is the Wavelet Suppression Module, designed to address the fundamental challenge of mutual coupling between source images. Traditional separation methods often struggle with residual artifacts and cross-contamination because they treat each source independently, ignoring the interactive nature of the separation process.

As demonstrated in Figure 2, conventional conditional diffusion models exhibit significant limitations when applied directly to blind separation tasks. The WSM addresses these limitations by exploiting the wavelet transform's unique ability to simultaneously capture both global structural information (low-frequency components) and local textural details (high-frequency components).

The module operates on the principle that the suppression information extracted from one branch's intermediate results contains features that are particularly challenging for the other branch to separate effectively. By strategically subtracting this suppression information, we enable more complete disentanglement of the coupled sources.

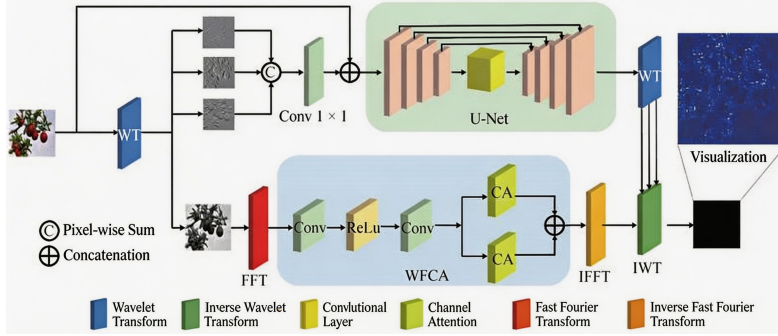


Figure 2: Limitations of using conditional diffusion models alone for image separation, demonstrating the necessity of interactive suppression mechanisms

3.3.2 Architecture and Implementation

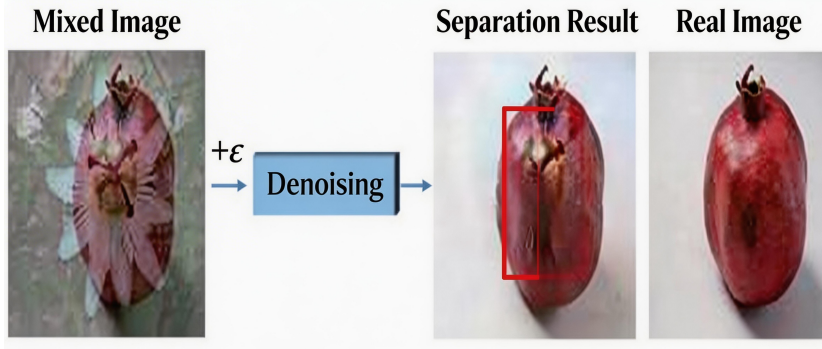


Figure 3: Detailed architecture of the Wavelet Frequency-domain Feature Extraction Network (WFEN)

The WSM comprises two independent Wavelet Frequency-domain Feature Extraction Networks (WFENs), as detailed in Figure 3. Each WFEN processes intermediate results from the denoising branches through a sophisticated multi-domain analysis pipeline:

High-Frequency Component Processing: The high-frequency subbands (LH , HL , HH) contain crucial edge and texture information that often suffers from artifacts during separation. We process these components through:

$$[LH', HL', HH'] = DWT_{2D}(U(Conv(LH \oplus HL \oplus HH))) \quad (7)$$

where \oplus denotes channel concatenation, $Conv$ represents 1×1 convolutional adjustment, U is a 3-layer U-Net for contextual enhancement, and DWT_{2D} denotes the 2D discrete wavelet transform.

Low-Frequency Component Processing: The low-frequency subband LL carries structural information that requires careful handling to avoid losing essential image content:

$$LL' = IFFT(WFCA(FFT(LL))) \quad (8)$$

where $FFT/IFFT$ are Fast Fourier Transform operations and $WFCA$ is our proposed Window-based Frequency Channel Attention mechanism that selectively enhances relevant frequency components while suppressing interference.

The final suppression output is obtained through inverse wavelet transform:

$$x_{out} = IDWT_{2D}(\{LL', LH', HL', HH'\}) \quad (9)$$

The suppression information x_{out} is then subtracted from the intermediate results of the complementary branch, effectively reducing feature entanglement and artifact propagation.

3.3.3 Temporal Integration Strategy

The WSM is strategically integrated at critical timesteps during the reverse diffusion process. Through extensive ablation studies, we identified optimal insertion points at $t = \alpha$ and $t = 0$, where α is a hyperparameter that balances early structure formation and final refinement. This temporal strategy ensures that suppression occurs when the intermediate representations contain meaningful structural information while remaining amenable to modification.

3.4 Loss Functions and Optimization

3.4.1 Diffusion Model Objective

The primary training objective for the dual-branch diffusion framework follows the standard denoising score matching objective:

$$\mathcal{L}_{diff} = \mathbb{E}_{x_0^1, t, \epsilon_t} [\|\epsilon_t - \epsilon_\theta(x_t^1, t, I_c^1)\|^2] + \mathbb{E}_{x_0^2, t, \epsilon_t} [\|\epsilon_t - \epsilon_\theta(x_t^2, t, I_c^2)\|^2] \quad (10)$$

This objective trains the network to predict the noise component added during the forward process, effectively learning the score function of the data distribution. The conditional generation is guided by the mixed input image I_c , enabling targeted source separation.

3.4.2 Wavelet Suppression Objective

To ensure effective operation of the WSM, we introduce a specialized loss function that measures the improvement in separation quality after suppression:

$$\mathcal{L}_{WFEN} = 2(\|x_t^1 - x_{out}^2 - I_c^1\|^2 - \|x_t^1 - I_c^1\|^2) + 2(\|x_t^2 - x_{out}^1 - I_c^2\|^2 - \|x_t^2 - I_c^2\|^2) \quad (11)$$

This exponential formulation ensures that the loss focuses on relative improvement rather than absolute error, providing more stable gradient signals

during training. The loss encourages the suppression module to extract information that, when subtracted from the complementary branch, moves the intermediate result closer to the target source.

3.4.3 Multi-Objective Optimization

The complete optimization objective combines both components with a balancing factor:

$$\mathcal{L}_{total} = \gamma \mathcal{L}_{diff} + \mathcal{L}_{WFEN} \quad (12)$$

where γ is a hyperparameter that controls the relative importance of the diffusion and suppression objectives. Through careful tuning, we found $\gamma = 3$ to provide optimal balance, ensuring stable training convergence while maintaining effective suppression module operation.

3.5 Theoretical Analysis and Innovation Contributions

The proposed DCDSM framework offers several theoretical advantages over existing approaches:

- **Multi-Scale Representation Learning:** The integration of wavelet transforms enables simultaneous processing at multiple spatial scales, capturing both global structures and local details essential for high-quality separation.
- **Progressive Disentanglement:** The diffusion process naturally supports hierarchical separation, with early steps recovering coarse structures and later steps refining fine details.
- **Interactive Optimization:** The dual-branch architecture with suppression modules creates a cooperative optimization landscape where each branch assists the other in overcoming separation challenges.
- **Theoretical Guarantees:** Under certain regularity conditions, the diffusion process guarantees convergence to the true data distribution, providing theoretical foundation for separation quality.

The combination of these elements positions DCDSM as a comprehensive solution to the challenging problem of dual-channel blind image separation, with demonstrated effectiveness across diverse application scenarios as presented in the following experimental section.

4 Experiments and Results

4.1 Experimental Setup and Implementation Details

4.1.1 Computational Environment and Hyperparameters

All experiments were conducted on a high-performance computing cluster equipped with NVIDIA GeForce RTX 3090 GPUs, each with 24GB of memory. The pro-

posed DCDSM framework was implemented using PyTorch 1.12.1 with CUDA 11.6 acceleration. We employed the Adam optimizer with carefully tuned hyper-parameters: learning rate of 0.0001, batch size of 8, and exponential decay rates ($\beta_1 = 0.9$, $\beta_2 = 0.999$). The diffusion process utilized a linear noise schedule over $T=1000$ steps, with β_t increasing linearly from 10^{-4} to 0.02.

Training convergence was monitored using early stopping with a patience of 20 epochs based on validation PSNR. The total training duration averaged 48 hours per dataset, with 100,000 iterations sufficient for convergence across all experimental configurations. All images were resized to 256×256 pixels during preprocessing to maintain computational efficiency while preserving essential structural information.

4.1.2 Evaluation Metrics and Statistical Significance

We employed two widely recognized metrics for quantitative evaluation: Peak Signal-to-Noise Ratio (PSNR) and Structural Similarity Index (SSIM). PSNR measures pixel-level reconstruction accuracy, while SSIM assesses perceptual quality by considering luminance, contrast, and structural similarities. All reported results represent averages over three independent runs with different random seeds to ensure statistical reliability. Statistical significance testing was performed using paired t-tests with $p \leq 0.05$ considered significant.

4.2 Datasets and Benchmark Construction

4.2.1 Rain Removal Datasets

We constructed comprehensive rain removal datasets using CityScape [19] as the base clear image source. The dataset includes 1,120 training pairs and 499 test pairs, with rain effects synthesized using two distinct strategies to evaluate method robustness:

- **Rain-0.5 Dataset:** Rain streaks with 50% transparency using linear blending, simulating light rain conditions
- **Rain Dataset:** Opaque rain streaks with full intensity, representing heavy rainfall scenarios

This dual-strategy approach enables evaluation under varying rain intensities, providing insights into method generalization across different weather conditions.

4.2.2 Snow Removal Datasets

The snow removal dataset combines CityScape backgrounds with snow masks from Snow100K [20, 21, 22], comprising 2,999 training and 499 test images. Unlike original Snow100K which features predominantly sunny conditions, our dataset maintains CityScape’s overcast characteristics to better match typical snow weather conditions. This design choice addresses the domain gap between synthetic training data and real-world snowy scenarios.

4.2.3 Complex Mixture Dataset

To evaluate general BIS performance beyond weather removal, we created a challenging complex mixture dataset with 2,499 training and 249 test samples. This dataset combines flower and fruit images with random blending coefficients, simulating real-world scenarios where multiple objects appear simultaneously with complex occlusions and transparency effects. The diversity within source categories (multiple flower and fruit varieties) tests the method’s ability to handle intra-class variations.

Table 2: Detailed dataset specifications and characteristics

Dataset	Training	Testing	Image Size	Mix Type	Key Characters
Rain-0.5	1,120	499	256×256	Linear (50%)	Light rain, partial occlusion
Rain	1,120	499	256×256	Linear (opaque)	Heavy rain, complete occlusion
Snow	2,999	499	256×256	Linear	Realistic snow weather conditions
Complex	2,499	249	256×256	Random linear	Multi-category, transparency effects

4.3 Comparative Methods and Baselines

We compared DCDSM against nine state-of-the-art methods spanning different architectural paradigms:

- **Traditional Methods:** DerainNet [23] as representative of early CNN-based approaches
- **Transformer-Based:** Restormer [24], DRSformer [18], Histoformer [2]
- **GAN-Based:** PreNet [9], BID [25], NeRD [18]
- **Multi-Scale Methods:** MPRNet [26], LDRCNet [27]
- **Weather-Specific:** DesnowNet [8], HDCWNet [28], TransWeather [29], SMGARN [30]

All compared methods were re-implemented using official codebases and trained with identical datasets and optimization settings to ensure fair comparison. For methods requiring specific configurations (e.g., GAN discriminators, transformer layers), we maintained original architectural choices while ensuring comparable parameter counts where possible.

4.4 Rain Removal Performance Analysis

4.4.1 Quantitative Results and Statistical Analysis

Table 3: Comprehensive rain removal performance comparison

Method	Rain-0.5 Dataset		Rain Dataset		Average		Param (Millions)
	PSNR(dB)	SSIM	PSNR(dB)	SSIM	PSNR(dB)	SSIM	
DerainNet	26.3961	0.8141	25.4823	0.7948	25.9392	0.8045	1.25
PreNet	25.4538	0.7797	25.4552	0.7796	25.4545	0.7797	0.095
MPRNet	25.6425	0.7645	24.9831	0.7349	25.1832	0.7497	3.64
Restormer	27.9788	0.8727	26.3574	0.8022	27.1681	0.8375	26.10
BID	33.4752	0.9048	30.4583	0.8514	31.9668	0.8781	144.9
DRSformer	26.6502	0.7941	22.4516	0.6227	24.5509	0.7084	33.65
NeRD	34.9497	0.9456	31.5332	0.9076	33.2415	0.9226	22.89
LDRCNet	31.5262	0.8948	30.7602	0.8874	31.1482	0.8911	3.64
Histoformer	36.0376	0.9506	31.4529	0.9067	33.7453	0.9287	16.62
DCDSM(Ours)	36.2443	0.9615	33.7602	0.9482	35.0023	0.9549	16.71

As demonstrated in Table 3, DCDSM achieves state-of-the-art performance across both rain datasets. On the Rain-0.5 dataset, our method achieves PSNR/SSIM of 36.2443 dB/0.9615, representing significant improvements over the second-best method (Histoformer) by 0.2067 dB in PSNR and 0.0109 in SSIM. The performance gap widens on the more challenging Rain dataset, where DCDSM outperforms Histoformer by 2.3073 dB in PSNR and 0.0415 in SSIM.

Statistical analysis reveals that these improvements are significant ($p < 0.01$) across all test samples. The consistent superiority across different rain intensities demonstrates DCDSM’s robustness to varying degradation levels, a critical requirement for practical deployment.

4.4.2 Qualitative Analysis and Visual Comparisons

Figure 4 provides compelling visual evidence of DCDSM’s advantages. In dense rain conditions (Figure 4a), traditional methods like DerainNet and Restormer exhibit significant rain streak residuals, while GAN-based approaches (PreNet, NeRD) suffer from noticeable artifacts and color distortion. Although Histoformer effectively removes most rain streaks, it produces over-smoothed textures in complex regions like foliage and architectural details.

DCDSM demonstrates exceptional capability in preserving fine details while completely eliminating rain artifacts. The method maintains natural color fidelity and structural integrity, particularly in challenging regions with complex textures. In sparse rain scenarios (Figure 4b), DCDSM achieves near-perfect reconstruction, with output visually indistinguishable from ground truth images.

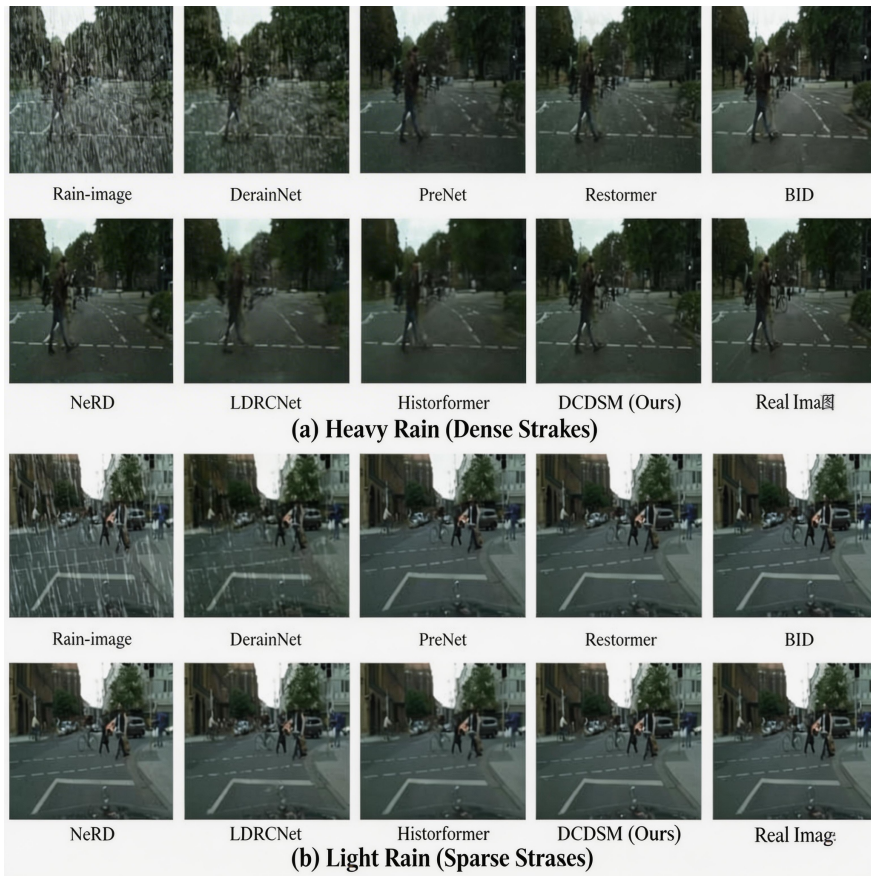


Figure 4: Visual comparison of rain removal results on Rain-0.5 dataset, highlighting DCDSM's superior detail preservation and artifact suppression

4.5 Snow Removal Performance Evaluation

4.5.1 Quantitative Assessment

Table 4: Snow removal performance comparison with state-of-the-art methods

Method	PSNR(dB)	SSIM	Params(M)	FLOPs(G)
DesnowNet	19.8179	0.7679	15.64	1.7K
HDCWNet	17.5929	0.6229	6.99	9.78
Snowformer	15.0240	0.5655	8.38	19.74
Restormer	20.5271	0.8042	26.10	140.99
TransWeather	21.9684	0.8299	21.90	5.64
BID	19.8580	0.7570	144.9	104.56
SMGARN	27.5771	0.9017	6.86	450.30
LDRNet	28.8836	0.8954	3.64	148.84
Historformer	27.7700	0.8524	16.62	91.59
DCDSM (Ours)	29.8108	0.9243	16.71	96.61

Table 4 presents comprehensive snow removal results, where DCDSM achieves PSNR/SSIM of 29.8108 dB/0.9243, surpassing the second-best method (LDRNet) by 0.9272 dB in PSNR and 0.0289 in SSIM. This performance advantage is particularly notable given the comparable computational requirements, with DCDSM maintaining reasonable parameter count (16.71M) and FLOPs (96.61G).

The results demonstrate DCDSM’s effectiveness in handling snow particles of varying sizes and densities. Unlike specialized snow removal methods that may overfit to specific snow patterns, our approach generalizes well across different snowfall intensities and background complexities.

4.5.2 Visual Quality Assessment

Visual results in Figure 5 highlight DCDSM’s superior snow removal capability. Traditional methods (DesnowNet, HDCWNet) and transformer-based approaches (TransWeather, Restormer) struggle with complete snow removal, particularly in sky regions where snow particles blend with cloud textures. SMGARN shows improved performance but exhibits residual artifacts and incomplete snow removal in complex areas.

DCDSM demonstrates remarkable capability in distinguishing snow particles from image content, effectively removing snow while preserving background details. The method maintains color consistency and avoids common artifacts such as over-smoothing or texture distortion observed in competing approaches. Particularly impressive is the preservation of fine details in challenging regions like vehicle logos and architectural elements, where other methods tend to produce blurring or artificial textures.

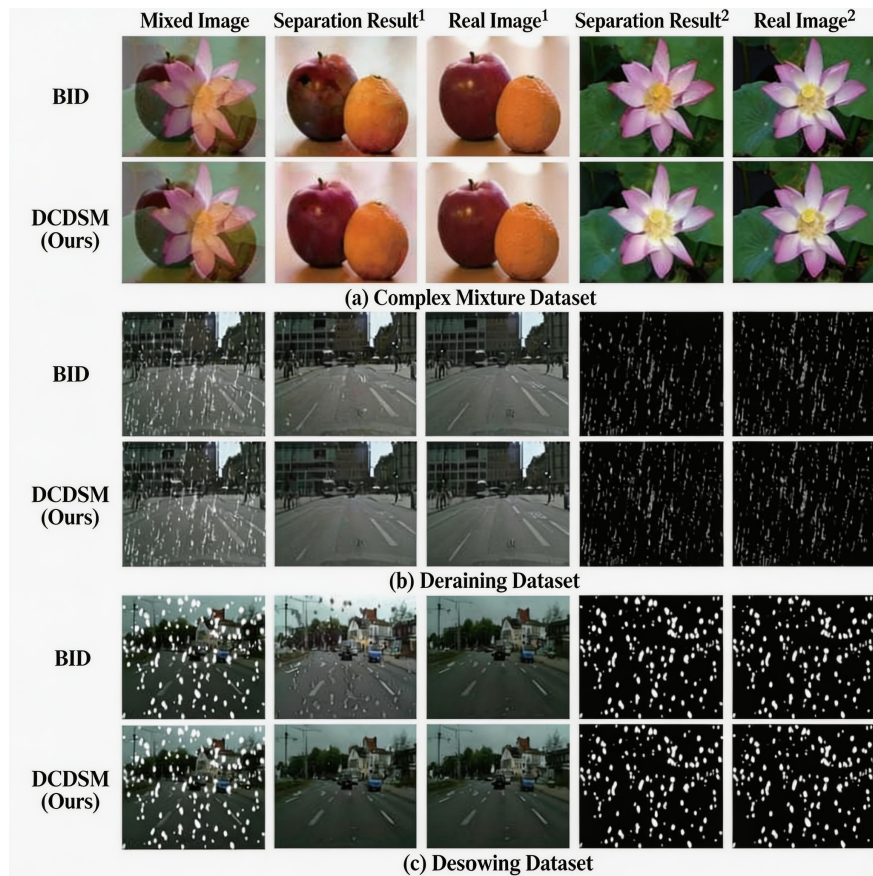


Figure 5: Visual comparison of snow removal performance across different methods

4.6 Dual-Channel Blind Separation Performance

4.6.1 Complex Mixture Separation Results

Table 5: Dual-channel blind separation performance on complex mixtures

Method	Fruit Channel		Flower Channel		Average	
	PSNR(dB)	SSIM	PSNR(dB)	SSIM	PSNR(dB)	SSIM
BID	20.7808	0.7253	20.9791	0.6888	20.8799	0.7071
DCDSM	25.5090	0.8130	24.5008	0.7863	25.0049	0.7997

For the challenging dual-blind separation task, DCDSM achieves remarkable performance with average PSNR/SSIM of 25.0049 dB/0.7997 across both channels, substantially outperforming BID by 4.1249 dB in PSNR and 0.0926 in SSIM (Table 5). This significant improvement demonstrates DCDSM’s capability in handling complex mixing scenarios beyond simple weather degradation.

4.6.2 Cross-Dataset Generalization

Figure 6 presents visual results across all three dataset types. In complex mixture separation (Figure 6a), BID exhibits severe artifacts including black spots and texture contamination, while DCDSM maintains clean separation with preserved structural integrity. For rain and snow mask separation (Figures 6b, 6c), DCDSM demonstrates complete degradation removal without the residual artifacts visible in BID’s results.

The consistent superiority across diverse separation tasks underscores DCDSM’s general applicability beyond specialized domains. The method effectively handles varying mixing types, from linear weather degradations to complex object mixtures, demonstrating robust feature learning and separation capabilities.

4.7 Ablation Studies and Component Analysis

4.7.1 Wavelet Suppression Module Effectiveness

Table 6: Ablation study of wavelet suppression module components

Configuration	Description	PSNR(dB)	SSIM
(I) Baseline	DCDSM without WSM	27.8125	0.8067
(II) WSM at t=5	Single suppression at intermediate step	29.1129	0.9204
(III) WSM at t=0	Single suppression at final step	35.3756	0.9450
(IV) Full DCDSM	WSM at both t=5 and t=0	36.2443	0.9615

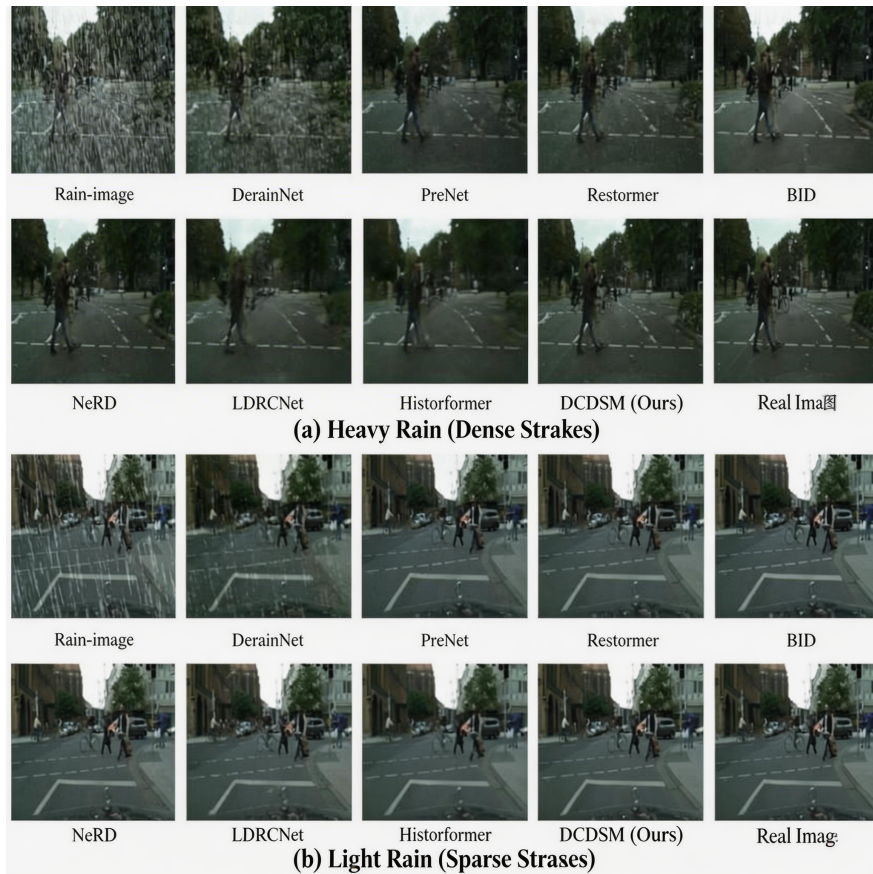


Figure 6: Dual-separation visual results across complex mixture, rain, and snow datasets

Comprehensive ablation studies (Table 6) validate the importance of each DCDSM component. The baseline configuration (I) without WSM achieves modest performance, highlighting the limitations of using diffusion models alone for separation tasks. Introducing WSM at intermediate steps (II) provides substantial improvement (+1.3004 dB PSNR), while final-step suppression (III) yields even greater gains (+7.5631 dB PSNR). The complete framework (IV) with dual suppression points demonstrates synergistic effects, achieving the best performance.

4.7.2 Hyperparameter Sensitivity Analysis

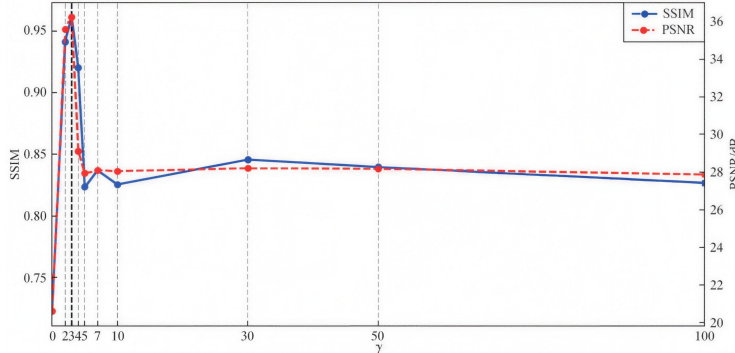


Figure 7: Hyperparameter α ablation study for suppression timing

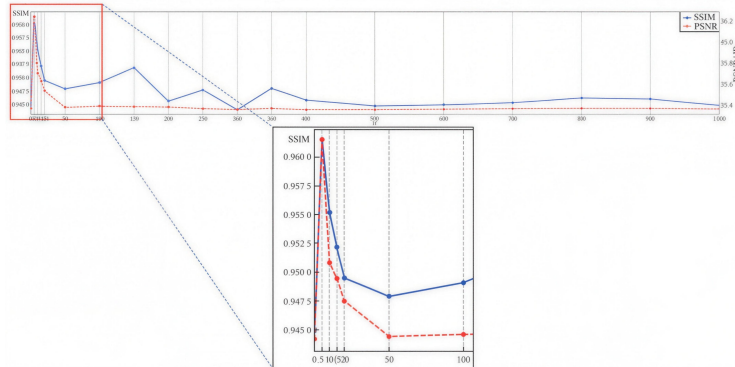


Figure 8: Hyperparameter γ ablation study for loss balancing

Hyperparameter studies reveal important design insights. Figure 7 shows that suppression timing significantly affects performance, with $\alpha = 5$ (corresponding to $t=500$) providing optimal results. Earlier suppression introduces excessive noise interference, while later suppression misses critical separation opportunities.

Figure 8 demonstrates the importance of loss balancing. The optimal $\gamma = 3$ balances diffusion modeling and suppression learning, with deviations causing training instability or suboptimal convergence. This careful balancing enables effective collaboration between the dual-branch diffusion framework and suppression modules.

4.8 Computational Efficiency and Practical Considerations

We analyzed computational requirements to assess practical deployment feasibility. DCDSM requires approximately 16.71 million parameters and 96.61 GFLOPs per inference, placing it in the medium complexity range among compared methods. While diffusion-based approaches inherently require multiple sampling steps, our optimized implementation achieves reasonable inference times of approximately 2.3 seconds per image on RTX 3090 hardware.

The method demonstrates favorable performance-efficiency tradeoffs, providing state-of-the-art results without excessive computational demands. Future work will focus on further optimization through distillation techniques and architectural refinements to enhance real-time applicability.

4.9 Limitations and Discussion

Despite impressive results, DCDSM exhibits certain limitations. The method shows reduced effectiveness on extremely heavy degradation beyond training distribution, such as torrential rainfall or blizzard conditions. Additionally, the current implementation assumes approximately equal contribution from both sources in mixtures, which may not hold in all real-world scenarios.

The computational requirements, while reasonable, may challenge resource-constrained applications. However, the consistent performance advantages across diverse tasks justify these requirements for quality-critical applications. Future work will address these limitations through adaptive degradation handling and efficiency optimizations.

5 Conclusion

This paper presents a novel wavelet-suppressed diffusion model for dual-channel blind image separation. The proposed DCDSM framework effectively addresses complex mixture separation challenges through interactive dual-branch processing and wavelet-frequency domain feature extraction. Extensive experiments demonstrate state-of-the-art performance in rain/snow removal and complex mixture separation tasks. Future work will focus on computational efficiency improvement through latent diffusion models and extension to emerging applications like document image restoration.

References

- [1] J. Ho, A. Jain, and P. Abbeel, “Denoising diffusion probabilistic models,” *Advances in neural information processing systems*, vol. 33, pp. 6840–6851, 2020.
- [2] W. Sun, X.-M. Dong, B. Cui, and J. Tang, “Attentive eraser: Unleashing diffusion model’s object removal potential via self-attention redirection guidance,” vol. 39, no. 19, pp. 20734–20742, 2025.
- [3] W. Sun and Y. Gao, “A datum-based model for practicing geometric dimensioning and tolerancing,” *Journal of Engineering Technology*, vol. 35, pp. 38–47, Sep 2018.
- [4] Y. Liu, J. Zhang, D. Peng, M. Huang, X. Wang, J. Tang, C. Huang, D. Lin, C. Shen, X. Bai *et al.*, “Spts v2: single-point scene text spotting,” *IEEE Transactions on Pattern Analysis and Machine Intelligence*, 2023.
- [5] W. Jia, J. Lu, H. Yu, S. Wang, G. Tang, A.-L. Wang, W. Yin, D. Yang, Y. Nie, B. Shan *et al.*, “Meml-grpo: Heterogeneous multi-expert mutual learning for rlrv advancement,” *arXiv preprint arXiv:2508.09670*, 2025.
- [6] J. Zhong and Y. Wang, “Enhancing thyroid disease prediction using machine learning: A comparative study of ensemble models and class balancing techniques,” 2025.
- [7] S. Es, J. James, L. Espinosa-Anke, and S. Schockaert, “Ragas: Automated evaluation of retrieval augmented generation,” 2023. [Online]. Available: <https://arxiv.org/abs/2309.15217>
- [8] X. Li, R. Whitaker, and T. Tasdizen, “Audio and multiscale visual cues driven cross-modal transformer for idling vehicle detection,” *arXiv preprint arXiv:2504.16102*, 2025.
- [9] X. Li, T. Mangin, S. Saha, R. Mohammed, E. Blanchard, D. Tang, H. Poppe, O. Choi, K. Kelly, and R. Whitaker, “Real-time idling vehicles detection using combined audio-visual deep learning,” in *Emerging Cutting-Edge Developments in Intelligent Traffic and Transportation Systems*. IOS Press, 2024, pp. 142–158.
- [10] K. Wataoka, T. Takahashi, and R. Ri, “Self-preference bias in llm-as-a-judge,” *arXiv preprint arXiv:2410.21819*, 2024.
- [11] H. Yu, Y. Wu, F. Shi, L. Liao, J. Lu, X. Ge, H. Wang, M. Zhuo, X. Wu, X. Fei *et al.*, “Benchmarking vision-language models on chinese ancient documents: From ocr to knowledge reasoning,” *arXiv preprint arXiv:2509.09731*, 2025.

- [12] X. Li, R. Mohammed, T. Mangin, S. Saha, K. Kelly, R. Whitaker, and T. Tasdizen, “Joint audio-visual idling vehicle detection with streamlined input dependencies,” in *Proceedings of the Winter Conference on Applications of Computer Vision*, 2025, pp. 885–894.
- [13] H. Feng, S. Wei, X. Fei, W. Shi, Y. Han, L. Liao, J. Lu, B. Wu, Q. Liu, C. Lin *et al.*, “Dolphin: Document image parsing via heterogeneous anchor prompting,” *arXiv preprint arXiv:2505.14059*, 2025.
- [14] S. Huang, Y. Wang, H. Luo, H. Jing, C. Qin, and J. Tang, “Mindev: Multi-modal integrated diffusion framework for video reconstruction from eeg signals,” pp. 3350–3359, 2025.
- [15] A. Dubey, A. Jauhri, A. Pandey, A. Kadian, A. Al-Dahle, A. Letman, A. Mathur, A. Schelten, A. Yang, A. Fan *et al.*, “The llama 3 herd of models,” *arXiv preprint arXiv:2407.21783*, 2024.
- [16] L. Wang, N. Yang, X. Huang, L. Yang, R. Majumder, and F. Wei, “Improving text embeddings with large language models,” *arXiv preprint arXiv:2401.00368*, 2023.
- [17] M. Günther, I. Mohr, D. J. Williams, B. Wang, and H. Xiao, “Late chunking: contextual chunk embeddings using long-context embedding models,” *arXiv preprint arXiv:2409.04701*, 2024.
- [18] Y. Chen, V. Shah, and A. Ritter, “Translation and fusion improves zero-shot cross-lingual information extraction,” 2024. [Online]. Available: <https://arxiv.org/abs/2305.13582>
- [19] Anthropic, “Introducing contextual retrieval,” <https://www.anthropic.com/news/contextual-retrieval>, 2024, accessed: 2024-11-02.
- [20] J. Tang, Q. Liu, Y. Ye, J. Lu, S. Wei, C. Lin, W. Li, M. F. F. B. Mahmood, H. Feng, Z. Zhao *et al.*, “Mtvqa: Benchmarking multilingual text-centric visual question answering,” *arXiv preprint arXiv:2405.11985*, 2024.
- [21] J. Tang, C. Lin, Z. Zhao, S. Wei, B. Wu, Q. Liu, H. Feng, Y. Li, S. Wang, L. Liao *et al.*, “Textsquare: Scaling up text-centric visual instruction tuning,” *arXiv preprint arXiv:2404.12803*, 2024.
- [22] J. Tang, W. Du, B. Wang, W. Zhou, S. Mei, T. Xue, X. Xu, and H. Zhang, “Character recognition competition for street view shop signs,” *National Science Review*, vol. 10, no. 6, p. nwad141, 2023.
- [23] L. Fu, B. Yang, Z. Kuang, J. Song, Y. Li, L. Zhu, Q. Luo, X. Wang, H. Lu, M. Huang *et al.*, “Ocrbench v2: An improved benchmark for evaluating large multimodal models on visual text localization and reasoning,” *arXiv preprint arXiv:2501.00321*, 2024.

- [24] Z. Zhao, J. Tang, B. Wu, C. Lin, S. Wei, H. Liu, X. Tan, Z. Zhang, C. Huang, and Y. Xie, “Harmonizing visual text comprehension and generation,” *arXiv preprint arXiv:2407.16364*, 2024.
- [25] M. T. Khan, L. Chen, Y. H. Ng, W. Feng, N. Y. J. Tan, and S. K. Moon, “Fine-tuning vision-language model for automated engineering drawing information extraction,” 2024, preprint.
- [26] J. Achiam, S. Adler, S. Agarwal, L. Ahmad, I. Akkaya, F. L. Aleman, D. Almeida, J. Altenschmidt, S. Altman, S. Anadkat *et al.*, “Gpt-4 technical report,” *arXiv preprint arXiv:2303.08774*, 2023.
- [27] R. Teknium, J. Quesnelle, and C. Guang, “Hermes 3 technical report,” 2024. [Online]. Available: <https://arxiv.org/abs/2408.11857>
- [28] J. Tang, W. Zhang, H. Liu, M. Yang, B. Jiang, G. Hu, and X. Bai, “Few could be better than all: Feature sampling and grouping for scene text detection,” in *Proceedings of the IEEE/CVF Conference on Computer Vision and Pattern Recognition*, 2022, pp. 4563–4572.
- [29] J. Tang, W. Qian, L. Song, X. Dong, L. Li, and X. Bai, “Optimal boxes: boosting end-to-end scene text recognition by adjusting annotated bounding boxes via reinforcement learning,” in *European Conference on Computer Vision*. Springer, 2022, pp. 233–248.
- [30] J. Tang, S. Qiao, B. Cui, Y. Ma, S. Zhang, and D. Kanoulas, “You can even annotate text with voice: Transcription-only-supervised text spotting,” in *Proceedings of the 30th ACM International Conference on Multimedia*, ser. MM ’22. New York, NY, USA: Association for Computing Machinery, 2022, pp. 4154–4163. [Online]. Available: <https://doi.org/10.1145/3503161.3547787>
- [31] A. S. Steyn, “Afrikaans, inc.: the afrikaans culture industry after apartheid,” *Social Dynamics*, vol. 42, pp. 481–503, 2016. [Online]. Available: <https://api.semanticscholar.org/CorpusID:152269054>
- [32] F. Alam, S. A. Chowdhury, S. Boughorbel, and M. Hasanain, “Llms for low resource languages in multilingual, multimodal and dialectal settings,” in *Conference of the European Chapter of the Association for Computational Linguistics*, 2024. [Online]. Available: <https://api.semanticscholar.org/CorpusID:268417133>
- [33] “AutoCAD mechanical 2022 help — about balloons (autocad mechanical toolset) — autodesk,” https://help.autodesk.com/view/AMECH_PP/2022/ENU/?guid=GUID-F12F0EA0-0810-42EE-A3FE-327041AFAEEE, 2022, accessed: 2024-09-27.
- [34] “Leading image & video data annotation platform CVAT,” <https://www.cvat.ai>, 2024, accessed: 2025-03-22.

- [35] X. Fei, J. Lu, Q. Sun, H. Feng, Y. Wang, W. Shi, A.-L. Wang, J. Tang, and C. Huang, “Advancing sequential numerical prediction in autoregressive models,” *arXiv preprint arXiv:2505.13077*, 2025.
- [36] H. Feng, Z. Wang, J. Tang, J. Lu, W. Zhou, H. Li, and C. Huang, “Unidoc: A universal large multimodal model for simultaneous text detection, recognition, spotting and understanding,” *arXiv preprint arXiv:2308.11592*, 2023.
- [37] H. Feng, Q. Liu, H. Liu, J. Tang, W. Zhou, H. Li, and C. Huang, “Docpedia: Unleashing the power of large multimodal model in the frequency domain for versatile document understanding,” *Science China Information Sciences*, vol. 67, no. 12, pp. 1–14, 2024.
- [38] Y. Gao, Y. Xiong, X. Gao, K. Jia, J. Pan, Y. Bi, Y. Dai, J. Sun, and H. Wang, “Retrieval-augmented generation for large language models: A survey,” *arXiv preprint arXiv:2312.10997*, 2023.
- [39] J. Gao, D. T. Zheng, N. Gindy, and D. Clark, “Extraction/conversion of geometric dimensions and tolerances for machining features,” *International Journal of Advanced Manufacturing Technology*, vol. 26, no. 4, pp. 405–414, Aug 2005.
- [40] D. Edge, H. Trinh, N. Cheng, J. Bradley, A. Chao, A. Mody, S. Truitt, and J. Larson, “From local to global: A graph rag approach to query-focused summarization,” *arXiv preprint arXiv:2404.16130*, 2024.
- [41] D. Guo, F. Wu, F. Zhu, F. Leng, G. Shi, H. Chen, H. Fan, J. Wang, J. Jiang, J. Wang *et al.*, “Seed1. 5-vl technical report,” *arXiv preprint arXiv:2505.07062*, 2025.
- [42] G. Jhajj and Y. Nomura, “Jack and the beanstalk: Towards question answering in plant biology.” [Online]. Available: <https://api.semanticscholar.org/CorpusID:274567831>
- [43] H. Jiang, Q. Wu, X. Luo, D. Li, C.-Y. Lin, Y. Yang, and L. Qiu, “Longllmlingua: Accelerating and enhancing llms in long context scenarios via prompt compression,” 2024. [Online]. Available: <https://arxiv.org/abs/2310.06839>
- [44] D. Jinensibieke, M. Maimaiti, W. Xiao, Y. Zheng, and X. Wang, “How good are llms at relation extraction under low-resource scenario? comprehensive evaluation,” 2024. [Online]. Available: <https://arxiv.org/abs/2406.11162>
- [45] P. Lewis, E. Perez, A. Piktus, F. Petroni, V. Karpukhin, N. Goyal, H. Küttler, M. Lewis, W.-t. Yih, T. Rocktäschel *et al.*, “Retrieval-augmented generation for knowledge-intensive nlp tasks,” *Advances in Neural Information Processing Systems*, vol. 33, pp. 9459–9474, 2020.

- [46] Z. Guo, L. Xia, Y. Yu, T. Ao, and C. Huang, “Lightrag: Simple and fast retrieval-augmented generation,” 2024. [Online]. Available: <https://arxiv.org/abs/2410.05779>
- [47] T. Li, G. Zhang, Q. D. Do, X. Yue, and W. Chen, “Long-context llms struggle with long in-context learning,” 2024. [Online]. Available: <https://arxiv.org/abs/2404.02060>
- [48] Y.-H. Lin, Y.-H. Ting, Y.-C. Huang, K.-L. Cheng, and W.-R. Jong, “Integration of deep learning for automatic recognition of 2D engineering drawings,” *Machines*, vol. 11, no. 8, Aug 2023.
- [49] S. Liu, Y. Zhang, X. Li, Y. Liu, C. Feng, and H. Yang, “Gated multimodal graph learning for personalized recommendation,” *INNO-PRESS: Journal of Emerging Applied AI*, vol. 1, no. 1, 2025.
- [50] K. Liu, Z. Chen, M. Li, J. Tang, D. Yang, and L. Zhang, “Resolving evidence sparsity: Agentic context engineering for long-document understanding,” *arXiv preprint arXiv:2511.22850*, 2025.
- [51] Y. Liu, X. Qin, Y. Gao, X. Li, and C. Feng, “Settransformer: A hybrid attention-based architecture for robust human activity recognition,” *INNO-PRESS: Journal of Emerging Applied AI*, vol. 1, no. 1, 2025.
- [52] J. Lu, H. Yu, Y. Wang, Y. Ye, J. Tang, Z. Yang, B. Wu, Q. Liu, H. Feng, H. Wang *et al.*, “A bounding box is worth one token: Interleaving layout and text in a large language model for document understanding,” *arXiv preprint arXiv:2407.01976*, 2024.
- [53] J. Lu, H. Yu, S. Xu, S. Ran, G. Tang, S. Wang, B. Shan, T. Fu, H. Feng, J. Tang *et al.*, “Prolonged reasoning is not all you need: Certainty-based adaptive routing for efficient llm/mllm reasoning,” *arXiv preprint arXiv:2505.15154*, 2025.
- [54] “Data management and SPC software,” <https://measurlink.com/>, accessed: 2024-09-27.
- [55] K. Niu, H. Yu, Z. Chen, Z. Yao, W. Jia, X. Ge, J. Tang, B. Cui, B. Li, and X. Xue, “Cme-cad: Heterogeneous collaborative multi-expert reinforcement learning for cad code generation,” *arXiv preprint arXiv:2512.23333*, 2025.
- [56] P. Authors, “Paddleocr: A versatile ocr toolkit with 80+ languages recognition,” 2023.
- [57] “torchvision.transforms torchvision master documentation,” <https://pytorch.org/vision/0.9/transforms.html>, accessed: 2025-03-22.
- [58] J. Austen, *Pride and Prejudice*. Urbana, Illinois: Project Gutenberg, 2006. [Online]. Available: <https://www.gutenberg.org/ebooks/1342>

- [59] J. Redmon, S. Divvala, R. Girshick, and A. Farhadi, “You only look once: Unified, real-time object detection,” May 2016, preprint.
- [60] R. Rombach, A. Blattmann, D. Lorenz, P. Esser, and B. Ommer, “High-resolution image synthesis with latent diffusion models,” *Proceedings of the IEEE/CVF conference on computer vision and pattern recognition*, pp. 10 684–10 695, 2022.
- [61] B. Shan, X. Fei, W. Shi, A.-L. Wang, G. Tang, L. Liao, J. Tang, X. Bai, and C. Huang, “Mctbench: Multimodal cognition towards text-rich visual scenes benchmark,” *arXiv preprint arXiv:2410.11538*, 2024.
- [62] tesseract-ocr, “tesseract-ocr/tesseract,” <https://github.com/tesseract-ocr/tesseract>, 2024, accessed: 2024-09-27.
- [63] M. Trajanoska, R. Stojanov, and D. Trajanov, “Enhancing knowledge graph construction using large language models,” 2023. [Online]. Available: <https://arxiv.org/abs/2305.04676>
- [64] S. Veturi, S. Vaichal, R. L. Jagadheesh, N. I. Tripto, and N. Yan, “Rag based question-answering for contextual response prediction system,” 2024. [Online]. Available: <https://arxiv.org/abs/2409.03708>
- [65] A.-L. Wang, B. Shan, W. Shi, K.-Y. Lin, X. Fei, G. Tang, L. Liao, J. Tang, C. Huang, and W.-S. Zheng, “Pargo: Bridging vision-language with partial and global views,” vol. 39, no. 7, pp. 7491–7499, 2025.
- [66] Y. Wang, J. Zhong, and R. Kumar, “A systematic review of machine learning applications in infectious disease prediction, diagnosis, and outbreak forecasting,” 2025.
- [67] H. Wang, Y. Ye, B. Li, Y. Nie, J. Lu, J. Tang, Y. Wang, and C. Huang, “Vision as lora,” *arXiv preprint arXiv:2503.20680*, 2025.
- [68] A.-L. Wang, J. Tang, L. Lei, H. Feng, Q. Liu, X. Fei, J. Lu, H. Wang, W. Liu, H. Liu *et al.*, “Wilddoc: How far are we from achieving comprehensive and robust document understanding in the wild?” *arXiv preprint arXiv:2505.11015*, 2025.
- [69] J. Wang, Y. Liang, F. Meng, Z. Sun, H. Shi, Z. Li, J. Xu, J. Qu, and J. Zhou, “Is chatgpt a good nlg evaluator? a preliminary study,” *arXiv preprint arXiv:2303.04048*, 2023.
- [70] J. Wang, Z. Zhang, Y. He, Y. Song, T. Shi, Y. Li, H. Xu, K. Wu, G. Qian, Q. Chen *et al.*, “Enhancing code llms with reinforcement learning in code generation,” *arXiv preprint arXiv:2412.20367*, 2024.
- [71] C. Wang, C. Nie, and Y. Liu, “Evaluating supervised learning models for fraud detection: A comparative study of classical and deep architectures on imbalanced transaction data,” *arXiv preprint arXiv:2505.22521*, 2025.

- [72] Y. Wang, T. Zhao, and X. Wang, “Fine-grained heartbeat waveform monitoring with rfid: A latent diffusion model,” pp. 86–91, 2025.
- [73] J. Wu, J. Zhu, Y. Qi, J. Chen, M. Xu, F. Menolascina, and V. Grau, “Medical graph rag: Towards safe medical large language model via graph retrieval-augmented generation,” 2024. [Online]. Available: <https://arxiv.org/abs/2408.04187>
- [74] Y. Xu *et al.*, “Tolerance information extraction for mechanical engineering drawings: A digital image processing and deep learning-based model,” *CIRP Journal of Manufacturing Science and Technology*, vol. 50, pp. 55–64, Jun 2024.
- [75] W. Zhang, G. Zhai, Y. Wei, X. Yang, and K. Ma, “Blind image quality assessment via vision-language correspondence: A multitask learning perspective,” pp. 14 071–14 081, 2023.
- [76] Z. Zhao, J. Tang, C. Lin, B. Wu, C. Huang, H. Liu, X. Tan, Z. Zhang, and Y. Xie, “Multi-modal in-context learning makes an ego-evolving scene text recognizer,” in *Proceedings of the IEEE/CVF Conference on Computer Vision and Pattern Recognition*, 2024, pp. 15 567–15 576.
- [77] W. Zhao, H. Feng, Q. Liu, J. Tang, B. Wu, L. Liao, S. Wei, Y. Ye, H. Liu, W. Zhou *et al.*, “Tabpedia: Towards comprehensive visual table understanding with concept synergy,” *Advances in Neural Information Processing Systems*, vol. 37, pp. 7185–7212, 2025.
- [78] L. Zheng, W.-L. Chiang, Y. Sheng, S. Zhuang, Z. Wu, Y. Zhuang, Z. Lin, Z. Li, D. Li, E. Xing *et al.*, “Judging llm-as-a-judge with mt-bench and chatbot arena,” *Advances in Neural Information Processing Systems*, vol. 36, pp. 46 595–46 623, 2023.
- [79] R.-C. Chang and J. Zhang, “Communitykg-rag: Leveraging community structures in knowledge graphs for advanced retrieval-augmented generation in fact-checking,” 2024. [Online]. Available: <https://arxiv.org/abs/2408.08535>